The corresponding propagators are easily found to be

$$\langle\psi^r\bar{\psi}_s\rangle=[24m^2(p^2-m^2)]^{-1}\{(\gamma p+m)\ \mathrm{tr}[(\gamma p+m)\Gamma_s(\gamma p-m)\Gamma^r]+2(\gamma p+m)\Gamma_s(\gamma p-m)\Gamma^r(\gamma p+m)\}$$
$$+[72m^2]^{-1}\{\gamma p\ \mathrm{tr}[\Gamma_s\Gamma^r]+2\ \mathrm{tr}[\gamma p\Gamma_s\Gamma^r]+2\gamma p\Gamma_s\Gamma^r-2\Gamma_s\gamma p\Gamma^r+2\Gamma_s\Gamma^r\gamma p\}+[8m]^{-1}\{\mathrm{tr}[\Gamma_s\Gamma^r]+2\Gamma_s\Gamma^r\}.$$

Similarly, for the spin-$(\frac{1}{2})$ field we may write

$$\Phi'_{[\alpha\beta]\gamma}=(2\sqrt{2})^{-1}(\beta^{-1})_{\alpha\beta}\psi_\gamma+(2\sqrt{2})^{-1}(\sigma_{\mu 5}\beta^{-1})_{\alpha\beta}\psi^{\mu 5}\gamma+(2\sqrt{2})^{-1}(\gamma_5\beta^{-1})_{\alpha\beta}\psi^5\gamma,$$

and find for the propagators

$$\langle\psi^r\bar{\psi}_s\rangle_+=[12m^2(p^2-m^2)]^{-1}\{(\gamma p+m)\ \mathrm{tr}[(\gamma p+m)\Gamma_s(\gamma p-m)\Gamma^r]-(\gamma p+m)\Gamma_s(\gamma p-m)\Gamma^r(\gamma p+m)\}$$
$$-[36m^2]^{-1}\{\gamma p\ \mathrm{tr}[\Gamma_s\Gamma^r]-4\ \mathrm{tr}[\gamma p\Gamma_s\Gamma^r]+\gamma p\Gamma_s\Gamma^r+5\Gamma_s\gamma p\Gamma^r+\Gamma_s\Gamma^r\gamma p\}+[4m]^{-1}\{\mathrm{tr}[\Gamma_s\Gamma^r]-\Gamma_s\Gamma^r\}.$$

The explicit evaluation of these propagators is straightforward but the result is not particularly illuminating, and we omit it. We note that the residues at the pole $p^2=m^2$ are identical with those of SDS, but that the contact terms are different. The asymptotic behavior for large p is no worse than linear.

PHYSICAL REVIEW VOLUME 139, NUMBER 3B 9 AUGUST 1965

Low-Energy K^--Meson Interactions in Hydrogen*

M. SAKITT,† T. B. DAY, R. G. GLASSER, AND N. SEEMAN
University of Maryland, College Park, Maryland and Naval Research Laboratory, Washington, D. C.

AND

J. FRIEDMAN, W. E. HUMPHREY, AND R. R. ROSS
Lawrence Radiation Laboratory, University of California, Berkeley, California

(Received 25 March 1965)

Low-energy K^--meson interactions in hydrogen are studied in the following channels:

$$K^-+p\rightarrow K^-+p,$$
$$K^-+p\rightarrow\Sigma^-+\pi^+,$$
$$K^-+p\rightarrow\Sigma^++\pi^-,$$

and cross sections, as a function of momentum, are presented in the region of 60–300 MeV/c K^- laboratory momentum. These cross sections, combined with existing data, are used to fit the zero-effective-range theory of Dalitz and Tuan. Two possible solutions are obtained; the preferred one agrees with previous higher energy data. The favored solution also suggests an S-wave bound state at 1410 MeV, which could be associated with the Y_0^* at 1405 MeV whose spin is still undetermined. Various properties of the two solutions are presented for K^-p interactions and K_2^0p interactions.

I. INTRODUCTION

DURING the past several years there have been several theoretical investigations of low-energy $\bar{K}N$ interactions. Jackson and Wyld,[1] and Dalitz and Tuan[2] have both developed an S-wave zero-effective-range formalism, taking into account the Coulomb interactions and mass-difference effects. Humphrey and Ross[3] measured the cross sections, in the various channels, at K^- laboratory momentum below 275 MeV/c, and using the Dalitz and Tuan formalism determined two possible sets of scattering lengths, $HR1$ and $HR2$. The favored solution, $HR1$, predicts a positive phase angle between the $T=1$ and $T=0$ amplitudes for $\Sigma\pi$ production from K^-P, while $HR2$ predicts a negative phase angle. Higher energy data[4] seem to imply a negative phase angle.[5] Attempts to explain K^-D interactions in terms of $\bar{K}N$ scattering lengths have been made[6–8] and seem to yield better agreement with $HR2$ than with $HR1$. Faced with these problems, it seemed interesting to redo the low-energy experiment with higher statistics.

* Work supported in part by the U. S. Atomic Energy Commission.

† Based in part on a Ph.D. dissertation submitted to the University of Maryland, 1965. Present address: Brookhaven National Laboratory, Upton, New York.

[1] J. D. Jackson, D. G. Ravenhall and H. W. Wyld, Nuovo Cimento **10**, 834 (1958).

[2] R. H. Dalitz and S. F. Tuan, Ann. Phys. **10**, 307 (1960).

[3] W. E. Humphrey and R. R. Ross, Phys. Rev. **127**, 1305 (1962).

[4] M. B. Watson, M. Ferri-Luzzi, and R. D. Tripp, Phys. Rev. **131**, 2248 (1963).

[5] T. Akiba and R. H. Capps, Phys. Rev. Letters **8**, 457 (1962).

[6] T. B. Day, G. A. Snow, and J. Sucher, Nuovo Cimento **14**, 637 (1959).

[7] R. Chand and R. H. Dalitz, Ann. Phys. (N. Y.) **20**, 1 (1962).

[8] A. K. Bhatia and J. Sucher, Phys. Rev. **132**, 855 (1963).

The exposure for this experiment was made in the 15-in. Berkeley hydrogen bubble chamber at the Bevatron. The low-energy beam used was similar to that used by Humphrey and Ross.[9] A vertical magnetic field of about 10 kG was maintained in the chamber. Approximately 45 000 pictures were taken, with about 1.25 K^-'s per picture.

II. ANALYSIS OF DATA

A. Cutoffs and Corrections for the Data

A small portion of the chamber, where the beam entered, was used to identify, by means of ionization and curvature, the K^-. This led to a sample unbiased with respect to the type of interaction the K^- made in the central fiducial volume. Events found were measured on conventional digitized microscopes. Measurements were spatially reconstructed and constrained to obey energy and momentum conservation by the PACKAGE program. The PACKAGE and EXAMIN system have been described in detail by Humphrey and Rosenfield[10]

In order for an event to be accepted in the experiment, the K^- interaction vertex had to occur inside the fiducial volume. The volume was determined so as to exclude events which either occurred in the region of the chamber which was used to identify the incoming K^- track in the scanning or occurred too close to a chamber wall to allow measurements on all tracks. The fiducial-volume test was performed on the events in the computer.

A total of 1567 elastic scatters, 449 Σ^- productions, and 322 Σ^+ productions were found.

1. In-Flight Σ Production

In order to eliminate the hard-to-measure events and make an easier separation between in-flight and at-rest events, two cuts were made on the Σ events. The projected length of the Σ was required to be greater than one millimeter. This made the collinearity test in the scan more meaningful and allowed the measurers to get a good determination of the Σ-track angles. The second cut was on the angle between the Σ and the incoming K^-. Since deviation from collinearity of the (Σ,π) angle vanishes as the (Σ,K^-) angle approaches either 0° or 180°, the backward and forward 20° cones were excluded from the experiment. Assuming that the hyperons were produced isotropically in the center-of-mass system, the probability of observing each event was calculated on the basis of these cuts and each event was weighted by the reciprocal of that probability.

TABLE I. Effects of cuts on data. For the elastic scatters, the number of events before cuts is not shown since they contain events in the region of $\cos\theta_{c.m.}>0.966$, where we do not evaluate the cross section.

p (MeV/c)	No. before cuts	No. after cuts	No. after corrections
(a) Σ^- hyperon production			
60– 80	25	21	28.22
80–100	39	29	38.80
100–120	51	38	48.49
120–140	54	44	54.92
140–160	51	42	55.64
160–180	46	34	43.91
180–200	50	39	49.68
200–220	48	44	55.50
220–240	26	21	26.68
240–260	36	30	38.29
260–280	19	16	21.45
280–300	15	15	19.70
(b) Σ^+ hyperon production			
60– 80	14	9	13.31
80–100	12	7	11.20
100–120	19	17	27.22
120–140	35	25	36.13
140–160	30	23	32.33
160–180	36	26	35.90
180–200	47	38	53.64
200–220	50	38	57.69
220–240	30	25	36.42
240–260	30	23	34.77
260–280	16	13	18.27
280–300	9	5	7.03
(c) Elastic scatters ($\cos\theta_{c.m.}\leq 0.966$)			
100–120		74	76.5
120–140		110	113.5
140–160		138	143.5
160–180		207	212.0
180–200		206	210.5
200–220		227	230.5
220–240		200	205.0
240–260		156	161.0
260–280		132	135.5
280–300		46	49.5

The number of events affected by the cuts and the corrections are displayed in Table I.

2. Elastic Scatters

In order to avoid the difficult problem of corrections for extremely forward angles of scattering, a cut of the cosine of the scattering angle in the center of mass was chosen. The cut was $\cos\theta_{c.m.}=0.966$, which was roughly 10° in the lab for the momentum range considered. With this cut, the dominance of the Coulomb scattering amplitude is seen in the angular distribution for momentum less than 200 MeV/c and at higher momentum the angular distribution becomes more isotropic, as expected.

In addition, corrections were made for events with $\cos\theta_{c.m.}$ greater than 0.85. These corrections were concerned with the difficulty of detecting forward-angle scatters if the plane of scatter tended to be vertical. If the plane of scatter made an angle of less than 30° with the vertical, the event was rejected. A correction

[9] N. Horwitz, J. J. Murray, R. R. Ross, and R. D. Tripp, University of California Radiation Laboratory Report No. UCRL-8269, 1958 (unpublished).

[10] W. E. Humphrey and A. H. Rosenfeld, Ann. Rev. Nucl. Sci. **13**, (1963).

of 3/2 was made for those events surviving that criterion. The effect of this cut is shown in Table I.

A cut on the laboratory momentum was chosen at 100 MeV/c, since the ability to detect a scatter strongly depends on both the length of recoil and the length of the secondary K. If the 100-MeV/c K back-scatters, it will give rise to a proton recoil 0.7 cm long, which is detectable. In addition, because of the turbulence in the chamber and the use of "coat-hangers" to reflect the light back up from the bottom of the chamber, distortion occasionally occurs. In tracks longer than several millimeters, these distortions can be distinguished from real scatters. Since the range of a 100-MeV/c K^- is about 1.5 cm, these distortion effects were eliminated.

B. Determination of Path Length and Cross Sections

1. Path Length

The K^- path length was determined by measuring every K^- meson in a randomly selected sample of one-fifth the total number of frames. Separate library and data tapes were prepared for this problem. The K mesons were measured as single tracks and no fitting was done. If a beam track had been previously measured, because it gave rise to an event of interest, then the fitted quantities of the K track were also put onto the path-length data tape.

The K meson beam was designed for a stopping run, but naturally a fraction of the K^- mesons just went through the chamber and another fraction interacted in flight. The momentum spectrum, at the entrance to the fiducial region, is shown in Fig. 1. When a good kinematical fit existed, we used the fitted quantities for the K^-, since the errors were significantly smaller. In addition, for unfitted tracks, we compared the values of momentum obtained by curvature with those obtained from range (assuming the K stopped). If the momentum from range was greater or within a standard deviation of that from curvature, we called the K over-

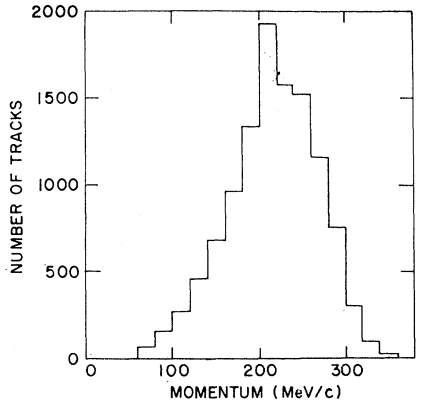

FIG. 1. Momentum distribution of a randomly selected sample of 1/5 the total number of K tracks at the entrance to fiducial volume.

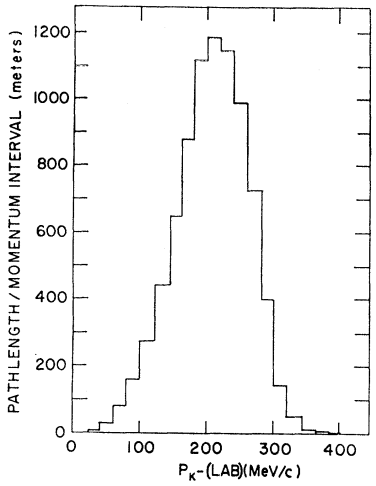

FIG. 2. Path-length distribution plotted as a function of K^- momentum in the laboratory.

stopped and assigned zero momentum to the end of the K track.

For each track, then, we had either a fitted momentum at the end, zero momentum at the end, or a curvature measurement at some point along the track. The value of momentum was then used to determine the momentum of the K when it entered our fiducial region. The K was then propagated along its track, until either the track ended or it left the region, and using energy-loss tables, the amount of length along the track in each momentum interval was determined. The resulting path-length distribution is shown in Fig. 2.

2. Cross Sections

Now that we have obtained an estimate of both the path length and the number of events of a particular type as a function of momentum, we can evaluate the cross section, σ. We define

$$\sigma_i{}^j=\frac{n_i{}^j}{l_i}\left(\frac{A}{\rho N_0}\right)=\frac{an_i{}^j}{l_i};\quad a=\frac{A}{\rho N_0},$$

where $(\rho N_0/A)$ is the number of protons per unit volume $(3.5\times10^{22}/\text{cm}^3)$, l_i is the observed K^- path length in the ith momentum bin, $n_i{}^j$ is the corrected number of interactions of the jth event type in the ith momentum bin, and $\sigma_i{}^j$ is the cross section for the production of event type j averaged over momentum bin i. The resulting cross sections are shown in Figs. 3–5. The variance for the cross section is obtained by

$$\delta\sigma_i\delta\sigma_j=\sigma_i\left\{\frac{1}{n_i}\langle\delta n_i\delta n_j\rangle\frac{1}{n_j}+\frac{1}{l_i}\langle\delta 1_i\delta 1_j\rangle\frac{1}{l_j}\right\}\sigma_j,$$

where $\langle\delta n_i\delta n_j\rangle$ and $\langle\delta l_i\delta l_j\rangle$ are the variances for the number of events observed and path length, respectively, taking into account both statistical counting errors and the effect of bin overlapping due to uncertainty in

TABLE II. Momentum dependence of the elastic cross section ($-1.0 \leq \cos\theta \leq 0.966$).

K^- lab momentum interval (MeV/c)	Experimental cross section (mb)	Variance matrix for experimental cross section (The symmetric elements have not been duplicated.) 100–120	120–140	140–160	160–180	180–200	200–220	220–240	240–260	260–280	280–300
100–120	87.29	104.77									
120–140	79.22	0.73	58.28								
140–160	69.61	0.77	0.70	36.24							
160–180	75.76	0.69	0.69	0.71	28.77						
180–200	59.09	0.39	0.41	0.49	0.67	17.66					
200–220	60.49	0.16	0.19	0.26	0.40	0.44	16.84				
220–240	55.69	0.06	0.05	0.08	0.15	0.21	0.45	16.25			
240–260	51.50	0.09	0.08	0.09	0.07	0.06	0.16	0.43	17.84		
260–280	58.06	0.09	0.07	0.09	0.10	0.05	−0.01	0.10	0.56	27.00	
280–300	38.27	0.07	0.05	0.06	0.07	0.05	0.03	−0.02	−0.00	0.57	32.21

TABLE III. Momentum dependence of the Σ^- cross section.

K^- lab momentum interval (MeV/c)	Experimental cross section (mb)	Variance matrix for experimental cross section (The symmetric elements have not been duplicated.) 60–80	80–100	100–120	120–140	140–160	160–180	180–200	200–220	220–240	240–260	260–280	280–300
60–80	113.5	917.96											
80–100	80.00	−73.71	347.96										
100–120	60.41	−10.70	−26.86	151.12									
120–140	41.97	−0.78	−5.00	−12.38	64.70								
140–160	29.14	0.60	−0.51	−2.30	−5.75	31.92							
160–180	16.64	0.41	0.09	−0.13	−1.20	−2.70	13.75						
180–200	14.60	0.29	0.15	0.15	−0.04	−0.43	−1.53	8.77					
200–220	15.35	0.25	0.15	0.15	0.08	−0.01	−0.33	−1.07	8.12				
220–240	7.83	0.14	0.08	0.08	0.05	0.03	−0.04	−0.23	−0.80	5.19			
240–260	12.68	0.18	0.12	0.11	0.08	0.05	0.02	−0.02	−0.20	−0.90	8.06		
260–280	9.40	0.11	0.07	0.07	0.05	0.03	0.02	0.01	−0.03	−0.21	−0.87	9.18	
280–300	16.17	0.26	0.17	0.16	0.11	0.08	0.04	0.03	0.03	−0.05	−0.43	−2.62	25.77

TABLE IV. Momentum dependence of the Σ^+ cross section.

K^- lab momentum interval (MeV/c)	Experimental cross section (mb)	Variance matrix for experimental cross section (The symmetric elements have not been duplicated.) 60–80	80–100	100–120	120–140	140–160	160–180	180–200	200–220	220–240	240–260	260–280	280–300
60–80	51.93	430.26											
80–100	23.58	−30.11	166.55										
100–120	33.87	−6.49	−22.43	111.36									
120–140	28.07	−0.75	−5.46	−10.07	48.08								
140–160	17.13	−0.15	−0.69	−1.91	−4.05	20.83							
160–180	13.66	0.02	0.01	−0.19	−0.58	−1.98	11.77						
180–200	17.05	0.16	0.11	0.11	0.05	−0.45	−1.43	11.87					
200–220	17.01	0.14	0.10	0.13	0.13	−0.02	−0.36	−1.55	11.91				
220–240	10.71	0.06	0.05	0.06	0.07	0.02	−0.03	−0.30	−1.20	7.67			
240–260	11.86	0.08	0.05	0.08	0.07	0.04	0.02	−0.04	−0.38	−1.14	9.66		
260–280	8.73	0.07	0.05	0.07	0.06	0.04	0.03	0.03	−0.04	−0.40	−1.40	9.70	
280–300	5.88	0.05	0.03	0.04	0.04	0.02	0.01	−0.01	−0.10	−0.27	−0.73	−1.54	13.99

momentum. The resulting variances are shown in Tables II-IV.

III. ANALYSIS OF EXPERIMENTAL RESULTS AND CONCLUSIONS

A. Test of S-Wave Assumption

In the fitting to the Dalitz-Tuan formalism, we shall assume that we can neglect the contributions of all partial waves above $l=0$. A test of the reasonableness of this assumption is the shape of the angular distribution, in the center of mass, of the production events. The angular distribution $N(\theta)$, with no angular momentum states contributing other than $l=0$ and 1, must be

$$N(\theta)=A+B\cos\theta+C\cos^2\theta,$$

where

$$A=|a|^2+|a_1-a_3|^2,$$
$$B=2\,\mathrm{Re}a^*(a_1+2a_3),$$
$$C=|a_1+2a_3|^2-|a_1-a_3|^2,$$

TABLE V. Fitting of angular distribution. $C1$ is the approximate confidence level. df is the number of degrees of freedom.

	Isotropic: A $df=7$		$A+B\cos\theta$ $df=6$				$A+B\cos\theta+C\cos^2\theta$ $df=5$				
	χ^2	$C1$	A	B	χ^2	$C1$	A	B	C	χ^2	$C1$
Σ^-, (60–300) MeV/c	9.74	20%	48.69	−4.15	8.38	20%	52.79	−3.62	−18.40	6.51	25%
Σ^+, (60–300) MeV/c	10.2	17%	36.86	−9.16	7.32	30%	36.57	−9.17	1.41	7.3	20%
Kp, (100–200) MeV/c	9.13	25%	76.91	6.80	8.03	25%	79.07	2.07	−12.08	7.51	18%
Kp, (200–300) MeV/c	6.43	45%	84.33	14.25	2.15	90%	85.24	11.96	−5.43	2.05	85%

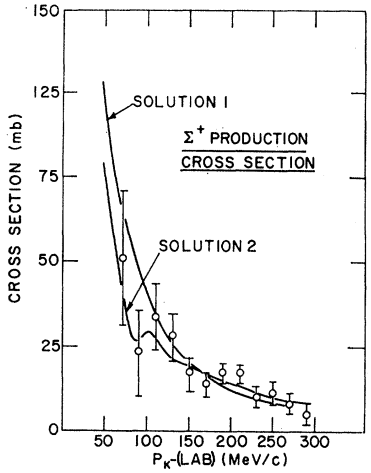

FIG. 3. Cross section for $K^-+p\rightarrow\Sigma^++\pi^-$. Solid curves are predicted values from solutions 1 and 2.

and a, a_1, and a_3 are the partial-wave amplitudes for S, $P_{1/2}$, and $P_{3/2}$ states, respectively.

In our case we expect the S wave to be dominant and therefore, as the $l=1$ part starts to appear, it will be easier to detect it first, by looking for a $\cos\theta$ term in the angular distribution.

The elastic scatters were numerous enough to be divided into two momentum intervals: 100–200 MeV/c and 200–300 MeV/c. The two resulting angular distributions are shown in Fig. 6. In the (100–200) MeV/c angular distribution, there is isotropic nulcear scattering with the additional Coulomb scattering present in the forward scattering region, i.e., $0.6\leq\cos\theta\leq0.8$.

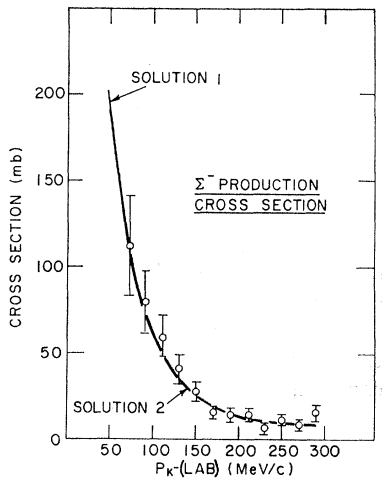

FIG. 4. Cross section for $K^-+p\rightarrow\Sigma^-+\pi^+$. Solid curves are predicted values from solutions 1 and 2.

The Coulomb contribution is noticeably less for the higher momentum angular distributions. In order to fit only the pure nuclear part of the scattering, the last bin, $0.6\leq\cos\theta\leq0.8$, was deleted. For the hyperon production events, in order to obtain sufficient statistics, all Σ^+ were grouped onto one graph, Fig. 7, and similarly for the Σ^- which are also shown in Fig. 7. The resulting four angular distributions were then fitted to an isotropic $A+B\cos\theta$, and $A+B\cos\theta+C\cos^2\theta$ distributions. The results of these fits are shown in Table V.

The fitting shows that there is no appreciable increase in the confidence level when higher terms than the constant one are included. These fits show that the data are consistent with the S-wave hypothesis.

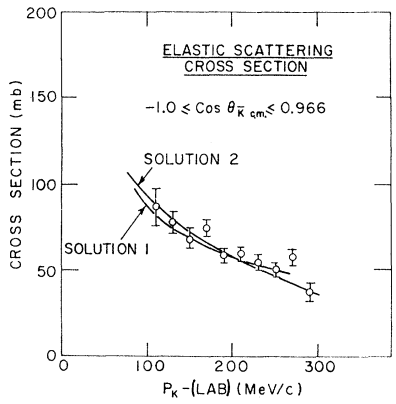

FIG. 5. Cross section for $K^-+p\rightarrow K^-+p$. Solid curves are predicted values from solutions 1 and 2.

B. Fitting to Dalitz-Tuan Formalism

Dalitz and Tuan[2] have described the low-energy S-wave $\bar{K}N$ interactions in terms of a zero-effective-range theory, including the effect of the Coulomb interaction and the $(\bar{K}^0,K^-)$ mass difference. Rather than go through the detailed arguments, we shall merely state the results of this approach:

$$\frac{d\sigma_{ce}(\theta)}{d\Omega}=\left|\frac{\csc^2(\theta/2)}{2Bk^2}\exp\left[\frac{2i}{kB}\ln\sin(\theta/2)\right]\right.$$
$$\left.+\frac{C^2}{2}\frac{[A_0(1-ik_0A_1)+A_1(1-ik_0A_0)]}{D}\right|^2, \quad (1)$$

$$\sigma_{ce}=\frac{\pi k_0C^2}{k}\left|\frac{A_0-A_1}{D}\right|^2, \quad (2)$$

$$\sigma_0=\frac{4\pi C^2}{k}\,\mathrm{Im}A_0\left|\frac{1-ik_0A_0}{D}\right|, \tag{3}$$

$$\sigma_1=\frac{4\pi C^2\,\mathrm{Im}A_1}{k}\left|\frac{1-ik_0A_0}{D}\right|, \tag{4}$$

where

$$D=1-i[k_0+C^2k(1-i\lambda)]\left(\frac{A_0+A_1}{D}\right)$$
$$-k_0[C^2k(1-i\lambda)]A_0A_1, \tag{5}$$

k is the center-of-mass wave number of K^-, k_0 is the center-of-mass wave number of $\bar{K}^0$, C^2 is the Coulomb penetration factor, $(2\pi/kB)[1-\exp(-2\pi/kB)]^{-1}$, B is the Bohr radius of K^-p system, A_0, A_1 are the complex scattering lengths for isotopic spin 0 and 1, λ is the function of k as defined by Dalitz and Tuan.[2] We can now relate the $(\Lambda\pi^0)$ amplitude to the $(\Sigma\pi)$ amplitude by a parameter ϵ, the ratio of the $(\Lambda\pi^0)$ production rate to the total hyperon rate in the isotopic spin one channel. At present there is no experimental evidence to indicate any rapid variation of ϵ up to laboratory momenta of 400 MeV/c.[3,4,11] We will take ϵ to be a constant. Thus

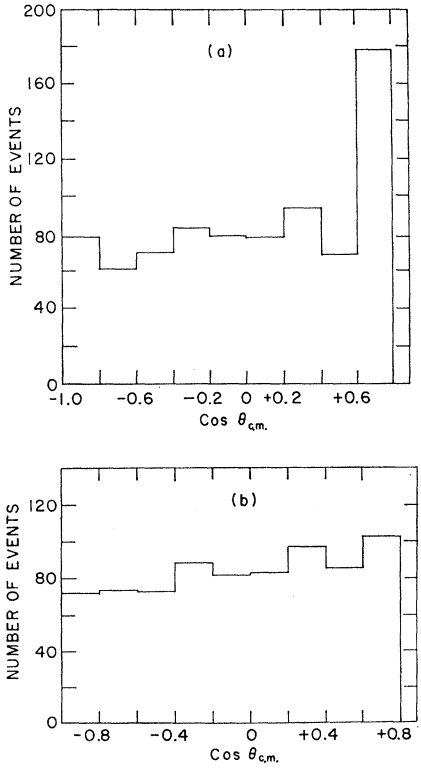

FIG. 6. Angular distribution for K^-p elastic scatters. $\mathrm{Cos}\theta_{c.m.}$ is the scattering angle in the center-of-mass system. (a) $100\leq P_k^{\mathrm{lab}}\leq 300$ MeV/c. (b) $200\leq P_k^{\mathrm{lab}}\leq 300$ MeV/c.

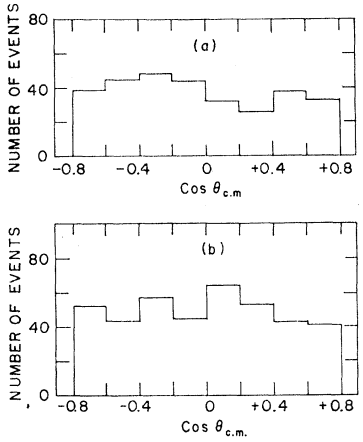

FIG. 7. Center-of-mass angular distributions with $60\leq P_k^{\mathrm{lab}}\leq 300$ MeV/c and $-0.8\leq\cos\theta_{c.m.}\leq+0.8$. (a) $K^-+p\rightarrow\Sigma^++\pi^-$. (b) $K^-+p\rightarrow\Sigma^-+\pi^+$.

we can write, using Clebsch-Gordan coefficients,

$$\sigma(K^-+p\rightarrow\Sigma^-+\pi^+)=\tfrac{1}{6}\sigma_0+\tfrac{1}{4}(1-\epsilon)\sigma_1$$
$$+[\tfrac{1}{6}\sigma_0\sigma_1(1-\epsilon)]^{1/2}\cos\phi,$$

$$\sigma(K^-+p\rightarrow\Sigma^++\pi^-)=\tfrac{1}{6}\sigma_0+\tfrac{1}{4}(1-\epsilon)\sigma_1$$
$$-[\tfrac{1}{6}\sigma_0\sigma_1(1-\epsilon)]^{1/2}\cos\phi,$$

$$\sigma(K^-+p\rightarrow\Sigma^0+\pi^0)=\tfrac{1}{6}\sigma_0,$$

and

$$\sigma(K^-+p\rightarrow\Lambda+\pi^0)=\tfrac{1}{2}\sigma_1\epsilon.$$

In addition to the above formulas we assume

(1) The scattering lengths A_0 and A_1 are independent of momentum.

(2) The momentum dependence of the phase angle between the $T=0$ and $T=1$ channels is given by[2]

$$\phi=\phi_{\mathrm{th}}+\arg\left(\frac{1-ik_0A_1}{1-ik_0A_0}\right), \tag{6}$$

where ϕ_{th} is the value of the phase angle at the $\bar{K}^0N$ threshold.

Since the capture reaction for K^-p takes place from the S wave,[12] we can use the relatively well-determined at-rest branching ratios. The ratio of Σ^-/Σ^+ production will accurately determine the value of ϕ at one point. It will be more convenient to define

$$\gamma=\Gamma(K^-+p\rightarrow\Sigma^-+\pi^+)/\Gamma(K^-+p\rightarrow\Sigma^+-\pi^-)$$

and use this parameter rather than the angle between the $T=1$ and $T=0$ $\Sigma\pi$ amplitudes. We now have a set of six parameters $(A_0,A_1,\epsilon,\gamma)$ which describe the low-energy $\bar{K}N$ interactions.

The above equations were used to calculate, as a function of the six parameters, theoretical values for all experimentally observed quantities which were in turn

[11] D. Luers, I. Mittra, W. Willis, and S. Yamamoto, Phys. Rev. 7, 255 (1961).

[12] T. B. Day, G. A. Show, and J. Sucher, Phys. Rev. Letters 3, 61 (1959).

TABLE VI. Measurements used in determining K^-p scattering lengths.

k	Physical quantity measured	No. of meas.	Tot. range of K^- lab momentum (MeV/c)	Reference
1	$\int_{-1.00}^{0.85} \frac{d\sigma_{el}}{d\Omega} d\Omega$	10	100–300	Present experiment
2	$\int_{0.85}^{0.90} \frac{d\sigma_{el}}{d\Omega} d\Omega$	10	100–300	Present experiment
3	$\int_{0.90}^{0.95} \frac{d\sigma_{el}}{d\Omega} d\Omega$	10	100–300	Present experiment
4	$\int_{0.95}^{0.966} \frac{d\sigma_{el}}{d\Omega} d\Omega$	10	100–300	Present experiment
5	$\sigma(K^-+p \to \bar{K}^0+n)$	7	100–275	HR (Ref. 3)
6	$\sigma(K^-+p \to \Sigma^-+\pi^+)$	12	60–300	Present experiment
7	$\sigma(K^-+p \to \Sigma^++\pi^-)$	12	60–300	Present experiment
8	$\Gamma(K^-+p \to \Sigma^-+\pi^+)/\Gamma(K^-+p \to \Sigma^++\pi^-)$	1	At rest	HR (Ref. 3)
9	$\frac{\Gamma(K^-+p \to \Lambda+\pi^0)}{\Gamma(K^-+p \to \Lambda+\pi^0)+\Gamma(K^-+p \to \Sigma^0+\pi^0)}$	1	At rest	HR (Ref. 3)
10	$\frac{\Gamma(K^-+p \to \Sigma^-+\pi^+)+\Gamma(K^-+p \to \Sigma^++\pi^-)}{\Gamma(K^-+p \to \Sigma^0+\pi^0)+\Gamma(K^-+p \to \Lambda+\pi^0)}$	1	At rest	HR (Ref. 3)
11	$\frac{\sigma(K^-+p \to \Lambda+\pi^0)}{\sigma(K^-+p \to \Lambda+\pi^0)+\sigma(K^-+p \to \Sigma^0+\pi^0)}$	4	100–260	Kim *et al.* (Ref. 13)
		78		

used to form a χ^2 defined by

$$\chi^2(A_0,A_1,\epsilon,\gamma)=\sum_{a,j,k}(\sigma_{aj}{}^T-\sigma_{aj}{}^M)(V^a)_{jk}{}^{-1}(\sigma_{ak}{}^T-\sigma_{ak}{}^M),$$

where V^a is the variance matrix for the experimental results of type a, $\sigma_{aj}{}^T$ is the theoretical cross section of class a, momentum bin j, $\sigma_{aj}{}^M$ is the measured cross section of class a, momentum bin j. The set of parameters which yield a minimum for χ^2 is our best estimate of the "true" parameters and the value of χ^2 at that minimum yields a confidence level for the fit. In addition, the shape of the χ^2 in the vicinity of the minimum yields an estimate for the error for the determined set of parameters.

The minimizing was carried out by a program called MINFUN.[10] This program, given the function χ^2 $(A_0,A_1,\epsilon,\gamma)$, performed two main tasks. The first task was that of exploring the six-dimensional space, skipping over small minima, and locating the promising regions where minima may be found. This was essentially a rough survey of the space. The second task was to hunt for the actual minimum in any specified region. It did this by evaluating the six-dimensional gradient and moving all the parameters in the direction necessary to minimize χ^2.

The momentum and angle regions for which measurements were made and used in the calculation of χ^2 are shown in Table VI. This experiment supplied the cross sections for both charged hyperon production and elastic scattering. The elastic scattering was divided as shown into four bins, depending on their scattering angle, so as to display more clearly the Coulomb nuclear inter-

TABLE VII. Previous scattering-length solutions.

Solution	a_0	b_0	a_1	b_1	γ	ϵ
a^-	−0.75	2.00	−0.85	0.21	2.15	0.41
b^+	1.15	2.00	0.70	0.25	2.15	0.41
a^+	0.05	1.10	1.45	0.35	2.15	0.41
b^-	−1.85	1.10	−0.10	0.65	2.15	0.41
*HR*1	−0.22	2.74	0.02	0.38	2.15	0.40
*HR*2	−0.59	0.96	1.20	0.56	2.04	0.39
*K*1	−0.65	1.54	−0.85	0.16	2.46	0.49
*K*2	−1.67	0.72	0.00	0.69	2.09	0.32

TABLE VIII. Values of the S-wave zero-effective-range parameters, yielding minima in χ^2.

Solution	A_0 (F) a_0	b_0	A_1 (F) a_1	b_1	γ (φ_m)	ϵ	χ^2 72 degrees of freedom	P (χ^2)
1[a]	−0.75	1.13	−0.85	0.15	2.19	0.48	88.6	8%
2[b]	−1.63	0.51	−0.19	0.44	2.11	0.31	76.0	38%

[a] Solution 1 used *HR*1 as starting point in search.
[b] Solution 2 used *HR*2 as starting point in search.

TABLE IX. Variance matrix for solution 1. (Symmetric elements have not been duplicated.)

	a_0	b_0	a_1	b_1	γ	ϵ
a_0	2.35×10^{-2}					
b_0	5.53×10^{-3}	2.24×10^{-2}				
a_1	-9.00×10^{-3}	2.08×10^{-3}	5.14×10^{-3}			
b_1	-3.61×10^{-3}	-1.45×10^{-3}	1.38×10^{-3}	9.72×10^{-4}		
γ	8.17×10^{-3}	1.05×10^{-3}	-3.66×10^{-3}	-6.50×10^{-3}	-1.33×10^{-2}	
ϵ	3.12×10^{-3}	8.53×10^{-3}	3.28×10^{-4}	-1.35×10^{-3}	-1.05×10^{-3}	6.34×10^{-3}

TABLE X. Variance matrix for solution 2. (Symmetric elements have not been duplicated.)

	a_0	b_0	a_1	b_1	γ	ϵ
a_0	4.25×10^{-3}					
b_0	-7.28×10^{-4}	2.25×10^{-3}				
a_1	-3.87×10^{-3}	1.24×10^{-3}	7.07×10^{-3}			
b_1	-1.03×10^{-3}	7.61×10^{-4}	2.47×10^{-3}	1.80×10^{-3}		
γ	-8.45×10^{-4}	-2.05×10^{-3}	2.23×10^{-3}	1.03×10^{-3}	1.36×10^{-2}	
ϵ	-8.60×10^{-4}	9.70×10^{-4}	1.25×10^{-3}	4.84×10^{-4}	-6.69×10^{-4}	1.22×10^{-3}

ference. The at-rest data and charge-exchange scattering are from the older Humphrey and Ross[3] experiment. The $\Lambda/(\Lambda+\Sigma^0)$ ratio as a function of momenta was taken from Kim *et al.*[13] We have 78 measurements from which we determine six parameters. Therefore, the fit will have 72 degrees of freedom.

In the earlier experiment of Humphrey and Ross,[3] four starting points were used in the search. These were the four solutions, calculated by Dalitz,[14] based on K^-P data at 175 MeV/c, and called a^-, a^+, b^-, and b^+. These four solutions and the two Humphrey and Ross solutions, $HR1$ and $HR2$, are shown in Table VII. Humphrey and Ross[3] found that solutions a^- and b^+ led to solution $HR1$, which had a confidence level of 48%, while solutions a^+, and b^- led to solution $HR2$, which had a confidence level of 8%.

Using $HR1$ and $HR2$ as our starting points, since they were based on more data than the original Dalitz solutions, we located two acceptable solutions. $HR1$ led to solution one ($S1$), with a confidence level of 8%, and $HR2$ led to solution two ($S2$), with a confidence level of 28%, which are shown in Table VIII, and their variances are shown in Tables IX and X. It is important to note that the variance matrices in Tables IX and X show that the errors are highly correlated and that simply looking at the diagonal errors as standard deviations for the propagation of errors can be quite misleading. The determined solutions $S1$ and $S2$ are different from the original starting points $HR1$ and $HR2$. The probability of making two measurements and obtaining the values $S1$ and $HR1$, or $S2$ and $HR2$, are both less than 0.19%. It is interesting to note that $S1$ is very close to the Dalitz a^- solution, while $S2$, which is the favored solution, is very close to the Dalitz b^- solution. Some very recent work of Kim[15] has led to scattering lengths, also shown in Table VII as $K1$ and $K2$, which are also very close to $S1$ and $S2$, respectively, with $K2$ also being the preferred solution.

The contributions of the various measurements to the final χ^2 are shown in Table XI.

TABLE XI. Specific contributions to final χ^2 for both solutions.

K (See Table 5.2)	Number of measurements	Solution 1	Solution 2
1	10	14.21	15.14
2	10	6.81	6.46
3	10	18.41	17.71
4	10	10.85	11.76
5	7	8.40	1.98
6	12	12.08	10.98
7	12	13.28	5.24
8	1	0.03	0.13
9	1	0.03	0.13
10	1	0.53	2.34
11	4	3.87	4.29

IV. PROPERTIES OF THE DALITZ-TUAN SOLUTIONS

A. Possible Bound-State Interpretations

Using the new sets of parameters $S1$ and $S2$, we have calculated the momentum dependence of the various cross sections and ratios. These quantities are shown in Tables XII and XIII.

It is interesting to note that the preferred solution $S2$ has a phase difference of $-93°$ at 275 MeV/c, while

[13] J. K. Kim, C. Alff, M. Nussbaum, and J. Schultz, Bull. Am. Phys. Soc. **9**, 1 (1964).

[14] R. H. Dalitz, Rev. Mod. Phys. **33**, 471 (1961).

[15] J. K. Kim, Phys. Rev. Letters **14**, 29 (1965).

TABLE XII. Properties of solution 1.

K^- lab momentum (MeV/c)	σ_{el} (mb)	σ_{ce} (mb)	σ_{Σ^-} (mb)	σ_{Σ^+} (mb)	Σ^-/Σ^+
47.5	352.3	0.0	201.9	103.5	1.95
67.5	132.5	0.0	121.2	68.8	1.76
87.5	96.7	0.0	78.6	54.6	1.44
107.5	83.0	9.0	50.0	37.6	1.33
127.5	75.7	9.2	36.4	28.1	1.29
147.5	70.4	8.5	27.6	22.1	1.25
167.5	65.8	7.6	21.5	17.8	1.21
187.5	61.7	6.7	17.2	1.48	1.17
207.5	57.9	5.8	14.0	12.4	1.13
227.5	54.5	5.1	11.6	10.6	1.09
247.5	51.2	4.5	9.7	9.2	1.05
267.5	48.3	3.9	8.1	8.0	1.02

$S1$ has a phase angle of $+89°$ at 275 MeV/c. $S2$ is now consistent with the phase angle of $-110°$ observed in the 400 MeV/c region,[4] and with the argument of Akiba and Capps[5] which shows that a negative phase angle at 400 MeV/c strongly suggests a negative phase angle at lower energies. The higher energy data is therefore consistent with $S2$ and inconsistent with $S1$.

It has been proposed by Dalitz and Tuan[16] that there may be an $S_{\frac{1}{2}}$ bound state of the $\bar{K}N$ system, below the $\bar{K}N$ threshold, which would appear as a $(\Sigma\pi)$ resonance with spin and parity $\frac{1}{2}^-$. Dalitz[17] has shown that this would be observable in the scattering lengths and in fact, when b is small and a is negative, the mass of the resonant state would be

$$E_r = M_p + M_k - (2\mu_k a^2)^{-1} \tag{7}$$

with a width

$$\tfrac{1}{2}\Gamma = b(\mu_k a^3), \tag{8}$$

where M_p is the mass of the proton, 938.2 MeV; M_k is the mass of the K^-, 493.9 MeV; μ_k is the $\bar{K}N$ reduced mass, 323.5 MeV; a is the real part of the scattering length; b is imaginary part of the scattering length.

TABLE XIII. Properties of solution 2.

K^- lab momentum (MeV/c)	σ_{el} (mb)	σ_{ce} (mb)	σ_{Σ^-} (mb)	σ_{Σ^+} (mb)	Σ^-/Σ^+
47.5	346.6	0.0	191.0	78.8	2.43
67.5	149.1	0.0	120.1	43.0	2.79
87.5	102.1	0.0	85.8	25.4	3.39
107.5	89.0	20.5	52.9	26.7	1.98
127.5	81.0	20.8	37.6	23.3	1.61
147.5	74.2	18.9	28.1	20.2	1.40
167.5	67.8	16.7	21.8	17.5	1.25
187.5	62.1	14.6	17.3	15.2	1.14
207.5	57.0	12.7	14.1	13.3	1.06
227.5	52.5	11.0	11.7	11.7	1.00
247.5	48.4	9.6	9.9	10.4	0.95
267.5	44.8	8.4	8.4	9.3	0.91

There is at present a resonance called Y_0^*, whose spin is undetermined, with $S=-1$, and $T=0$, located at 1405 MeV[18,19] with a width of either 50 MeV[18] or 35 ± 5 MeV.[19] Our favored solution $S2$ fulfills the requirement of large negative a_0 and small b_0 and yields resonance parameters

$$E_r = 1409.6 \pm 1.7 \text{ MeV}$$

and

$$\Gamma = 28.2 \pm 4.1 \text{ MeV}.$$

The position of the predicted resonance is remarkable close to the Y_0^*, but its width is somewhat smaller. These parameters, however, would be affected by the inclusion of an effective range. Still it suggests that, indeed, the Y_0^* is an $S_{\frac{1}{2}}$ bound state of the $\bar{K}N$.

B. Properties of the Solutions in $K_2^0 p$ Interactions

The $\bar{K}N$ scattering lengths, which we have determined, coupled with the known KN scattering lengths[20] can be used, as shown by Biswas,[21] to describe the nuclear scattering of neutral K mesons. The particular experiment of interest is the scattering of a K_2^0 beam in hydrogen. The initial state is an equal mixture of $S=1$ and $S=-1$ with the $S=-1$ component in a pure $T=1$ state, while the $S=1$ is itself an equal mixture of $T=0$ and $T=1$. This initial state can scatter at low energies into $K_2^0 p$, $K_1^0 p$, or be absorbed into $Y\pi$, where Y is a hyperon of $S=-1$. If we only consider S waves and expand the various scattering amplitudes by use of the zero-effective-range approximation, we obtain[21]

$$\sigma(K_1) = \pi \left| \frac{1}{2}\frac{a_1}{1-ika_1} + \frac{1}{2}\frac{a_0}{1-ika_0} - \frac{\bar{a}_1 + i\bar{b}_1}{1+k\bar{b}-ik\bar{a}_1} \right|^2,$$

$$\sigma(K_2) = \pi \left| \frac{1}{2}\frac{a_1}{1-ika_1} + \frac{1}{2}\frac{a_0}{1-ika_0} - \epsilon\frac{\bar{a}_1 + i\bar{b}_1}{1+b_1-ika_1} \right|^2,$$

$$\sigma(Y) = \frac{2\pi}{k}\frac{\bar{b}_1}{1+2k\bar{b}_1+k^2(\bar{a}_1^2+\bar{b}_1^2)},$$

where a_T is the real scattering length for $S=1$, an isotopic spin T, and $(\bar{a}_1+i\bar{b}_1)$ is the complex scattering length for $S=-1$ and $T=1$.

Using the $S=1$ scattering lengths,[20]

$$a_0 = 0.04 \text{ F}$$
$$a_1 = -0.31 \text{ F},$$

[16] R. H. Dalitz and S. F. Tuan, Phys. Rev. Letters 2, 425 (1959).
[17] R. H. Dalitz, Phys. Rev. Letters 6, 239 (1961).
[18] M. Alston, L. Alvarez, M. Ferro-Luzzi, A. Rosenfeld, H. Ticho and S. G. Wojcicki, in *Proceedings of the 1962 Annual International Conference on High-Energy Nuclear Physics at CERN*, (CERN Geneva, 1962), p. 311.
[19] G. Alexander, G. Kalbfleisch, D. Miller, and G. Smith, Phys. Rev. Letters 8, 447 (1962).
[20] N. J. Stenger, W. E. Slater, D. H. Stork, H. K. Ticho, G. Goldhaber, and S. Goldhaber, Phys. Rev. 134, B111 (1964).
[21] N. N. Biswas, Phys. Rev. 118, 866 (1960).

TABLE XIV. Theoretical K_2^0+p interactions for solution 1.

P_{lab} (MeV/c)	$\sigma_{K_2^0 p}$ (mb)	$\sigma_{K_1^0 p}$ (mb)	$\sigma_{Y\pi}$ (mb)
60	28.3	14.9	43.6
80	27.4	14.3	31.9
100	26.3	13.7	24.8
120	25.2	13.0	20.1
140	24.1	12.4	16.6
160	23.1	11.7	14.0
180	22.0	11.0	12.0
200	21.0	10.4	10.4
220	20.0	9.8	9.1
240	19.0	9.2	8.0
260	18.1	8.7	7.1
280	17.3	8.1	6.3
300	16.5	7.7	5.7

TABLE XV. Theoretical K_2^0+p interactions for solution 2.

P_{lab} (MeV/c)	$\sigma_{K_2^0 p}$ (mb)	$\sigma_{K_1^0 p}$ (mb)	$\sigma_{Y\pi}$ (mb)
60	8.4	5.1	117.9
80	8.1	4.8	84.2
100	7.8	4.6	64.3
120	7.6	4.3	51.1
140	7.3	4.1	41.9
160	7.1	3.9	35.1
180	6.9	3.7	29.9
200	6.9	3.7	29.9
200	6.7	3.5	25.9
220	6.5	3.3	22.6
240	6.4	3.1	20.0
260	6.2	3.0	17.8
280	6.0	2.8	15.9
300	5.9	2.7	14.4

we can now generate graphs for the various cross sections, which are shown in Tables XIV and XV.

There exist some experimental data, by Luers *et al.*[11] on the ratio

$$F=K_1^0/(\Lambda+2\Sigma^0)$$

at 240 MeV/c. They obtained the value $R=0.4\sim0.9$. $S1$ predicts $R=1.15$ and $S2$ predicts $R=0.16$. It has been shown by Akiba and Capps[5] that the inclusion of a small effective range can change this ratio at 240 MeV/c. Determination of this ratio at lower momenta would distinguish more clearly between the two solutions.

V. CONCLUSIONS

The S-wave zero-effective-range theory adequately describes the low-energy K^-—P interactions. The angular distributions obtained were all quite consistent with isotropic nuclear scattering. This experiment has produced, as a favored solution, a set of scattering lengths $S2$ which now agree with higher energy experiments[4] and can also be used to interpret the Y_0^* at 1405 MeV, as a possible S-wave bound state of the $\bar{K}N$ system.

While the determined solutions differ with the results of Humphrey and Ross,[3] they agree with the earlier results of Dalitz[14] and the recent results of Kim.[15] A possible source of systematic error in the earlier experiment[3] could be a small contamination of at-rest events among the inflight sample, which raised the $(\Sigma^0+\Lambda)$ production cross section in the low-momentum region. This would also explain the high cross section for $(\Sigma^0+\Lambda)$ production that they obtained.

The $\bar{K}N$ scattering lengths, along with the KN scattering lengths, have been used to describe the low-energy $K_2^0 p$ interactions, as was suggested by Biswas.[21] It would be very interesting to study, experimentally, the ratio $K_1^0/(\Lambda+2\Sigma^0)$ around 200 MeV/c, since the one existing point, at 240 MeV/c[11] seems to fall, with large errors, somewhere between the values predicted by $S1$ and $S2$.

It would also be useful to combine the world's data on K^-p at low energy and then apply a nonzero-effective-range formalism.[22]

ACKNOWLEDGMENTS

It is a pleasure to acknowledge the informative discussions and advice of Professor G. A. Snow. One of us (M. S.) would like to acknowledge the United States Steel Foundation for a two-year fellowship during the time of this work. We would also like to thank the high-energy-group scanners and measurers at the Lawrence Radiation Laboratory, University of Maryland, and the Naval Research Laboratory.

[22] G. L. Shaw and M. Ross, Phys. Rev. **126**, 814 (1962).